SAND2021-12649C

Experimental Modal Analysis of a Resonant Plate During a Mid-Field Pyroshock Replication Test

Tyler F. Schoenherr
Sandia National Laboratories[1]
P.O. Box 5800 - MS0346
Albuquerque, NM, 87185

David E. Soine
Sandia National Laboratories[1]
P.O. Box 5800 - MS0346
Albuquerque, NM, 87185

Bryan L. Witt
Sandia National Laboratories[1]
P.O. Box 5800 - MS0557
Albuquerque, NM, 87185

Abstract

Resonant plate and other resonant fixture shock techniques were developed in the 1980s at Sandia National Laboratories as flexible methods to simulate mid-field pyroshock for component qualification. Since that time, many high severity shocks have been specified that take considerable time and expertise to setup and validate. To aid in test setup and to verify the shock test is providing the intended shock loading, it is useful to visualize the resonant motion of the test hardware. Experimental modal analysis is a valuable tool for structural dynamics visualization and model validation. This work describes a method to perform experimental modal testing at pyroshock excitation levels, utilizing input forces calculated

[1]Sandia National Laboratories is a multi-mission laboratory managed and operated by National Technology and Engineering Solutions of Sandia, LLC., a wholly owned subsidiary of Honeywell International, Inc., for the U.S. Department of Energy's National Nuclear Security Administration under contract DE-NA-0003525.

via the SWAT-TEEM (Sum of Weighted Accelerations Technique-Time Eliminated Elastic Motion) method and the measured acceleration responses. The calculated input force and measured acceleration data are processed to estimate natural frequencies, damping, and scaled mode shapes of a resonant plate test system. The modal properties estimated from the pyroshock-level test environment are compared to a traditional low-level modal test. The differences between the two modal tests are examined to determine the nonlinearity of the resonant plate test system.

Keywords
SWAT, Resonant Plate, Modal Analysis, Force Reconstruction

1 Introduction

Testing components or subassemblies in the laboratory is a cheaper and faster alternative to testing an entire system in its field environments. In some instances, performing a field test of the environment is untenable. This is often true of high-level shock environments which a system may experience. One method the test laboratory imparts shock environments onto a system is via a resonant plate apparatus.

Sandia National Laboratories sometimes uses a resonant plate to create a two sided shock response that is a more representative shock environment than a one sided pulse. Photographs of a resonant plate test configuration are in Figure 1. This test setup requires that the plate be flexible so its resonance can amplify the motion of the unit under test which is bolted to the plate at a frequency range present in the field environment. This flexibility at resonance allows for uncontrollable, off-axis motion during the test. This is an issue as current environment specifications dictate that three orthogonal shock inputs are input separately to simulate one environment. Uncontrollable off-axis motion can cause damage in an off-axis direction that would inadvertently accumulate over the three hits.

One solution to produce a more realistic environment is to develop a test that meets shock environments in all directions simultaneously. Executing a single shot test instead of three separate tests eliminates the desire to suppress off-axis motion and is more representative of the actual environment. Executing one test instead of three also reduces the time in the laboratory, which increases the lab capacity. However, executing a single shot multi-axis test is difficult because there is little control over the test. The test fires a high speed projectile to impact the resonant plate. There is little control over the projectile besides the projectile speed, the programmer that the projectile hits to shape the input force, and the size of the projectile.

Due to the limited control the test facility has in modifying the shock input, the success of the multi-axis test is contingent on the pre-test design using a finite element model. Characterization and designs of multi-axis shock have been previously explored [6] [7] [9]. These efforts place high focus on the response of the base of the unit under test and the

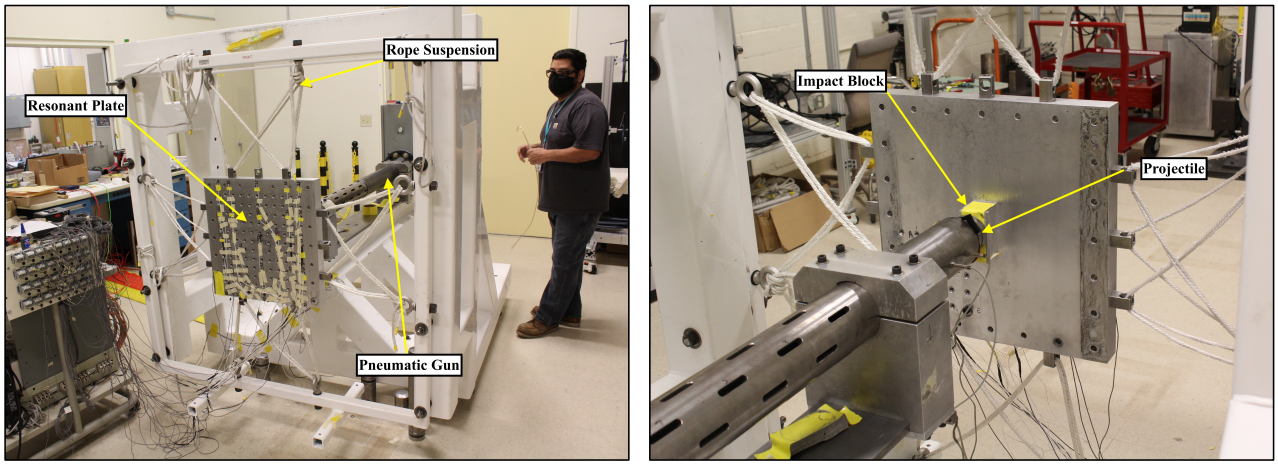

Figure 1: Photographs of the resonant plate test configuration without a test unit attached or damping bars.

unit under test itself. These efforts also explore moving both the unit under test and the impact location as possible means for designing a multi-axis test. Through these past efforts, it is clear that the use of a finite element model is critical in designing a test for a given multi-axis environment. Guessing on the test setup parameters in the lab is untenable due to the amount of time it takes to gather data on one test setup, assess the results, and formulate feedback to modify the resonant plate test setup.

Even with the use of a finite element model, information about the input force to the resonant plate must be known in order to produce a meaningful model response. Direct measurements are infeasible at such high force levels and short durations due to hardware limitations of load sensors. In the absence of a direct measurement of the input force, inverse methods are used to calculate the force that causes the measured accelerations. This is also a challenge as traditional inverse methods are susceptible to slight non-linearities in the structure. Nonlinearities are expected in the structure due to the bolting of the aluminum damping bars to the outer edge of the resonant plate. To further increase damping, a thin sheet of rubber is sandwiched between the damping bars and the resonant plate, all of which increases the nonlinearity of the system. These damping bars are added to make the test system damping closer to the fielded system. Another method to calculate the force is to use explicit models to determine these forces, however, modeling of the contact and programmer is difficult [4].

In order to determine the forces from the resonant plate tests, this body of work uses a spatial inverse method known as the Sum of Weighted Accelerations Technique - Time Eliminated Elastic Motions (SWAT-TEEM) [8]. This inverse method inverts spatial quantities (i.e. mode shapes) to calculate the causal force. Using mode shapes provides a buffer against most non-linearities as mode shapes are not as sensitive to system nonlinearities as natural frequency and damping. Furthermore, the SWAT-TEEM technique uses shapes acquired from the test which reduces errors in the basis shapes.

This paper details the force reconstruction process during the resonant plate environment. The paper then uses the forcing function in conjunction with the acceleration measurements to calculate modal parameters of the test hardware at shock levels. These modal parameters calculated at shock input levels are compared to the experimental modal results obtained at low input levels to determine the linearity of the system and to show if modal superposition theory is acceptable for resonant plate shock tests.

2 Theory and Background

This paper uses modal analysis theory and the force reconstruction algorithm known as the Sum of Weighted Acceleration Technique - Time Eliminated Elastic Motion (SWAT-TEEM) in order to compute the modal parameters of the resonant plate system. This section explains these topics in some detail to aid in digesting the analysis performed in this report, but the overview is not meant to be an exhaustive overview of the topics.

2.1 Modal Analysis

Modal analysis has been studied extensively and entire books have been written to aid in its understanding and application [1] [3] [5]. This section covers modal analysis at a high level so that the reader can understand its importance and how the system's modal parameters are extracted from the data acquired.
Modal analysis theory is first examined by producing the equations of motion of a generic structure. A structure's motion can be estimated by the 2$^{\text{nd}}$ order linear equations of motion

$$\mathbf{M}\ddot{\bar{x}} + \mathbf{C}\dot{\bar{x}} + \mathbf{K}\bar{x} = \bar{F}, \tag{1}$$

where $\mathbf{M}$ is the mass matrix, $\mathbf{C}$ is the damping matrix and $\mathbf{K}$ is the stiffness matrix of the system. The displacement of the structure can be described in the frequency domain and reorganized as

$$\frac{\ddot{\bar{x}}(j\omega)}{\bar{F}(j\omega)} = -\omega^2[-\omega^2\mathbf{M} + j\omega\mathbf{C} + \mathbf{K}]^{-1} \tag{2}$$

where j is the imaginary number. This form of the equations of motion is informative because it explicitly provides an input/output relationship between the displacement and the forcing function that caused the motion through a transfer function. This transfer function is specifically called a Frequency Response Function (FRF). Although the mass, damping, stiffness matrices of the finite element model can be calculated, these properties cannot be directly measured on a structure.

In order to be able to calculate and compare FRFs between the finite element model and the physical structure, an eigen analysis is performed on the structure. The eigen analysis in the finite element model calculates the eigenvalues and eigenvectors. The eigenvectors are calculated from the mass and stiffness matrices and are referred to in structural dynamics

as the mode shapes. These shapes are related to the displacement of the structure through a linear combination shown as

$$x_i \approx \sum_{m=1}^{n} \boldsymbol{\phi}_{im} q_m, \tag{3}$$

where $\boldsymbol{\phi}_{im}$ is the m^{th} mode shape of the structure at degree of freedom i and q_m is the modal coordinate corresponding to the participation of that mode shape in the displacement of the structure. The substitution shown in Eqn 3 is linear, however, it has been shown to be valid for systems with slight nonlinearities stemming from frictional contacts [2]. The modal substitution decouples the equations of motion shown in Eqn 1 and 2. As a result, FRFs can be calculated for both the finite element model and experimental data. These FRFs in the modal domain are written as

$$\frac{\ddot{x}_i(j\omega)}{F_k(j\omega)} \approx \sum_{m=1}^{n_{\text{mode}}} \frac{-\omega^2 \boldsymbol{\phi}_{im} \boldsymbol{\phi}_{km}}{-\omega^2 + 2j\omega\omega_m \boldsymbol{\zeta}_m + \omega_m^2}, \tag{4}$$

where ω_m is the m^{th} natural frequency of the structure and ζ_m is the modal damping corresponding to the m^{th} mode. This expression of the FRF matrix is computed element by element of the i^{th} response degree of freedom with respect to an input at the k^{th} degree of freedom. With the physical structure, a directly measured force and directly measured accelerations are obtained in order to calculate parts of the FRF matrix over the frequency range for which there is adequate excitation. The modal parameters of the structure are fit to the experimental FRFs using any number of methods.

In summary, modal analysis or eigen analysis is a method of transforming the data into a domain that allows for the comparison of finite element models and physical structures. Although the modal parameters are calculated from the finite element model, the experimental modal parameters need to be fit to the experimental FRFs.

2.2 Formulation of SWAT (Sum of Weighted Acceleration Technique)

The derivation of the SWAT-TEEM (Time Eliminated Elastic Motion) algorithm that is used to calculate the sum of the external forces begins with the 2^{nd} order linear equations of motion shown in Eq 1. The modal approximation shown in Eq 3 is substituted into Eq 1 to get

$$\mathbf{M}\boldsymbol{\phi}\ddot{\bar{q}} + \mathbf{C}\boldsymbol{\phi}\dot{\bar{q}} + \mathbf{K}\boldsymbol{\phi}\bar{q} = \bar{F}. \tag{5}$$

At this point, Eq 5 is premultiplied by the transpose of the rigid body modes, $\boldsymbol{\phi}_r^T$, to get

$$\boldsymbol{\phi}_r^T \mathbf{M}\boldsymbol{\phi}\ddot{\bar{q}} + \boldsymbol{\phi}_r^T \mathbf{C}\boldsymbol{\phi}\dot{\bar{q}} + \boldsymbol{\phi}_r^T \mathbf{K}\boldsymbol{\phi}\bar{q} = \boldsymbol{\phi}_r^T \bar{F}. \tag{6}$$

Because there is no internal damping or internal stiffness forces for the rigid body degrees of freedom, Eq 6 simplifies to

$$\boldsymbol{\phi}_r^T \mathbf{M}\boldsymbol{\phi}\ddot{\bar{q}} = \boldsymbol{\phi}_r^T \bar{F} \tag{7}$$

due to

$$\boldsymbol{\phi}_r^T \mathbf{C} = 0 \ \& \ \boldsymbol{\phi}_r^T \mathbf{K} = 0. \tag{8}$$

The physical degrees of freedom are substituted for the modal degrees of freedom using the relationship in Eq **??** into Eq 7 to get

$$\boldsymbol{\phi}_r^T \mathbf{M} \ddot{\bar{x}} = \boldsymbol{\phi}_r^T \bar{F}. \tag{9}$$

At this point a weighting matrix, $\boldsymbol{w}$, is defined as

$$\boldsymbol{w}^T = \boldsymbol{\phi}_r^T \mathbf{M}. \tag{10}$$

and substituted into Eq 9 to obtain

$$\boldsymbol{w}^T \ddot{\bar{x}} = \boldsymbol{\phi}_r^T \bar{F}. \tag{11}$$

To solve for the weighting vector, an assumption of the input force is made. In the case where the structure is impacted by an external force and then in a free state, there are no external forces after impact and the accelerations of the system, $\ddot{\bar{x}}_{fd}$, are assumed to decay exponential and Eq 11 after the impact simplifies to

$$\boldsymbol{w}^T \ddot{\bar{x}}_{fd} = 0. \tag{12}$$

To obtain a non-trivial solution, information about the rigid body modes needs to be included because they were not present in the free decayed response. The rigid body constraint is formed by post-multiplying Eq 10 by the rigid body shapes to get

$$\boldsymbol{w}^T \boldsymbol{\phi}_r = \boldsymbol{\phi}_r^T \mathbf{M} \boldsymbol{\phi}_r, \tag{13}$$

which can be simplified to

$$\boldsymbol{w}^T \boldsymbol{\phi}_r = M_r. \tag{14}$$

Where M_r is the modal mass of the rigid body modes. Equation 14 is added to Eq 12 to get

$$\boldsymbol{w}^T \left[\boldsymbol{\phi}_r \ \ddot{\bar{x}}_{fd} \right] = \left[M_r \ 0 \right]. \tag{15}$$

Equation 15 is solved for $\boldsymbol{w}^T$ and substituted back into Eq 11 to solve for the sum of external forces acting on the center of gravity written as

$$\left[M_r \ 0 \right] \left[\boldsymbol{\phi}_r \ \ddot{\bar{x}}_{fd} \right]^+ \ddot{\bar{x}} = \boldsymbol{\phi}_r^T \bar{F}. \tag{16}$$

Equation 15 is solved for the six weighting vectors, $\boldsymbol{w}^T$ in a constrained least squares problem with the rigid body shapes being the constraint. Because the pseudo-inverse includes the time domain response of the system which is a linear combination of the mode shapes, the mode shapes of the system do not need to be separately calculated as it does with the SWAT algorithm.

3 Modal Analysis of the Resonant Plate Test

A series of resonant plate tests were executed on the resonant plate with damping bars. The tests consist of different configurations of the test environment varying the projectile size, pressure of the pneumatic gun used to fire the projectile, and the thickness of the felt programmer. Each test configuration was repeated at least 4 times with nominally the same parameters. Each configuration is referred to as a set of runs. Each set of runs tested can be seen in Table 1.

The forces for each test run are estimated using the SWAT-TEEM method. The reconstructed force from run 56 is in Figure 2. From the environment, it is expected that the forcing function will look like a single sided pulse that starts and ends at zero. The force from run 56 is exactly that, however, there are some transient 'forces' after the main pulse. Knowing that the projectile disengages, it is known that the 'force' after 0.3 ms is erroneous and an artifact of not filtering the acceleration through the SWAT-TEEM process.

Knowledge of the shape of the input force is a means in determining the fidelity of the force reconstruction. Another means to test the integrity of the force reconstruction uses the conservation of momentum shown as

$$mv_0 + \int_{t_1}^{t_2} F(t)dt = mv_f \tag{17}$$

where m is the mass of the resonant plate system, v is the velocity of the resonant plate at the

Table 1: Table of the run sets and associated test parameters

Run Set Name	Test Runs	Pressure (psi)	Felt Thk (in)	Projectile Length (in)	Average Projectile Speed (ft/s)
Set 14	[14:17]	10	1/8" Grey	6"	21.5
Set 21	[21:27]	14	1/8" Grey	6"	28.1
Set 28	[28:31]	10	1/8" Grey	6"	21.3
Set 32	[32:35]	10	1/2" Grey	6"	21.4
Set 36	[36:39]	20	1/2" Grey	6"	35.7
Set 41	[41:47]	20	1" Grey	6"	36.0
Set 48	[48:51]	40	1" Grey	6"	53.5
Set 54	[54:57]	50	1" Grey	6"	59.8
Set 58	[58:61]	20	1" Grey	12"	23.9
Set 62	[62:65]	40	1" Grey	12"	37.1
Set 66	[66:68]	60	1" Grey	12"	46.1
Set 69	[69:72]	15	1/2" Grey	12"	19.5
Set 73	[73:76]	25	1/2" Grey	12"	27.8
Set 78	[78:81]	35	1/2" Grey	12"	34.1
Set 82	[82:85]	15	1/8" Grey	12"	19.1
Set 86	[86:91]	25	1/8" Grey	12"	27.5

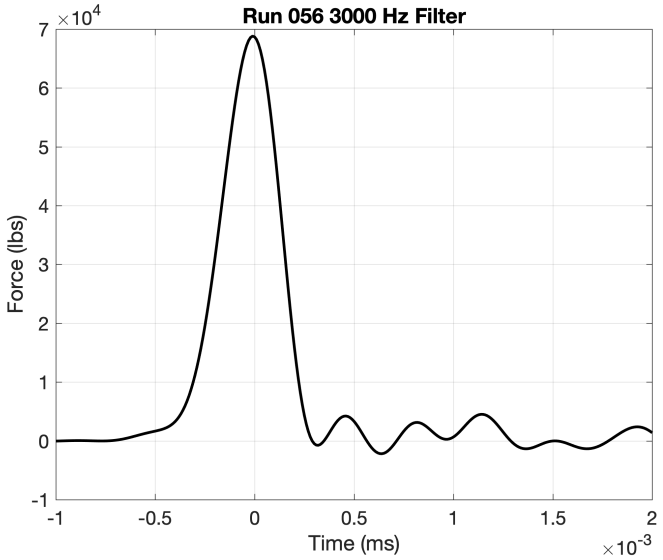

Figure 2: The reconstructed force from run 56 using the SWAT-TEEM algorithm and a 3kHz low pass filter.

initial, o, and final, f, moments, and $F(t)$ is the imparted force calculated by SWAT-TEEM. Because the initial velocity of the plate is zero for each of the runs, the final velocity of the plate could be calculated by dividing the impulse of the force by the mass of the plate.

The conservation of momentum is calculated for run 32 with the force passed through a 6 kHz low-pass filter. The data had the velocity of the plate calculated by integrating the accelerations. Although there is a spread of velocities of the integrated accelerometers due to rigid rotations and drift, the velocity calculated through the conservation of momentum is compared to the integrated measured accelerations. This integration of the measured accelerations is shown in Figure 3. The velocity of the plate calculated through the conservation of momentum is approximately the average of the integrated accelerations.

All of the forces calculated for the runs in Table 1 are transformed into the frequency domain for examination. Examination in the frequency domain allows for direct comparison between the different test parameters and to determine at which frequency bandwidths contain the majority of the energy. This concatenation of forces in the frequency domain can be seen in Figure 4.

Conclusions from examining the forces calculated are that the forces are relatively consistent when using the same test parameters: gun pressure, projectile size, felt thickness. Increasing the felt thickness does not significantly change the energy imparted by the projectile. When the felt thickness increases, the length of the pulse increases which reduces the high frequency force and increases the force at low frequencies.

Increasing the gun pressure and consequentially the projectile speed increases the energy of the impact and also reduces the pulse width of the impact. This provides an increase in force over all frequencies. However, that increase in force is not uniform over the frequency domain.

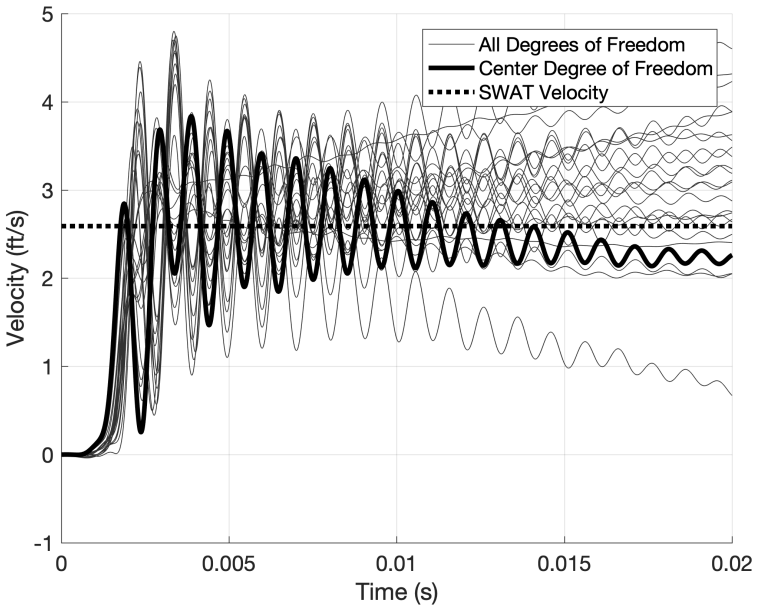

Figure 3: Integrated velocities from acceleration responses in run 32 with the velocity at the center of the plate bolded.

The last test parameter is the projectile size or weight. An increase in projectile weight provides a proportional increase in energy to the resonant plate. Another effect of increasing the weight of the projectile is a change in the pulse width of the force. This increases the forces for lower frequencies and reduces the force at higher frequencies.

With the force calculated at a known location, the acceleration data can be combined with the forcing function to calculate Frequency Response Functions (FRFs). From the FRFs, coherence of the averaged runs and modal parameters are calculated. Coherence and the FRF with respect to one degree of freedom is shown in Figure 5. The left plot in Figure 5 shows the FRF and coherence from averaging four resonant plate test runs of the same test parameters. The figure shows high coherence, greater than 0.9, for frequencies less than 4000 Hz except at frequencies of anti-resonances.

The right plot of Figure 5 averages four test runs of a low level hit with four test runs of a high level hit. The coherence is worse when compared to the coherence of data all at the same level, but it stays above 0.9 when less than 2500 Hz. This shows that although the system is not linear over different forcing levels, the nonlinearities are not significant enough to void modal superposition.

Modal parameters are fit to two discrete sets of data. One set is of low level impact data and the other is of high impact data. Six modes from the shock test are compared to the same modes acquired from traditional low-level experimental modal analysis testing. The forces from the low level modal test are about two orders of magnitude lower in peak force from the shock test. The mode shapes of the test display are difficult to interpret visually.

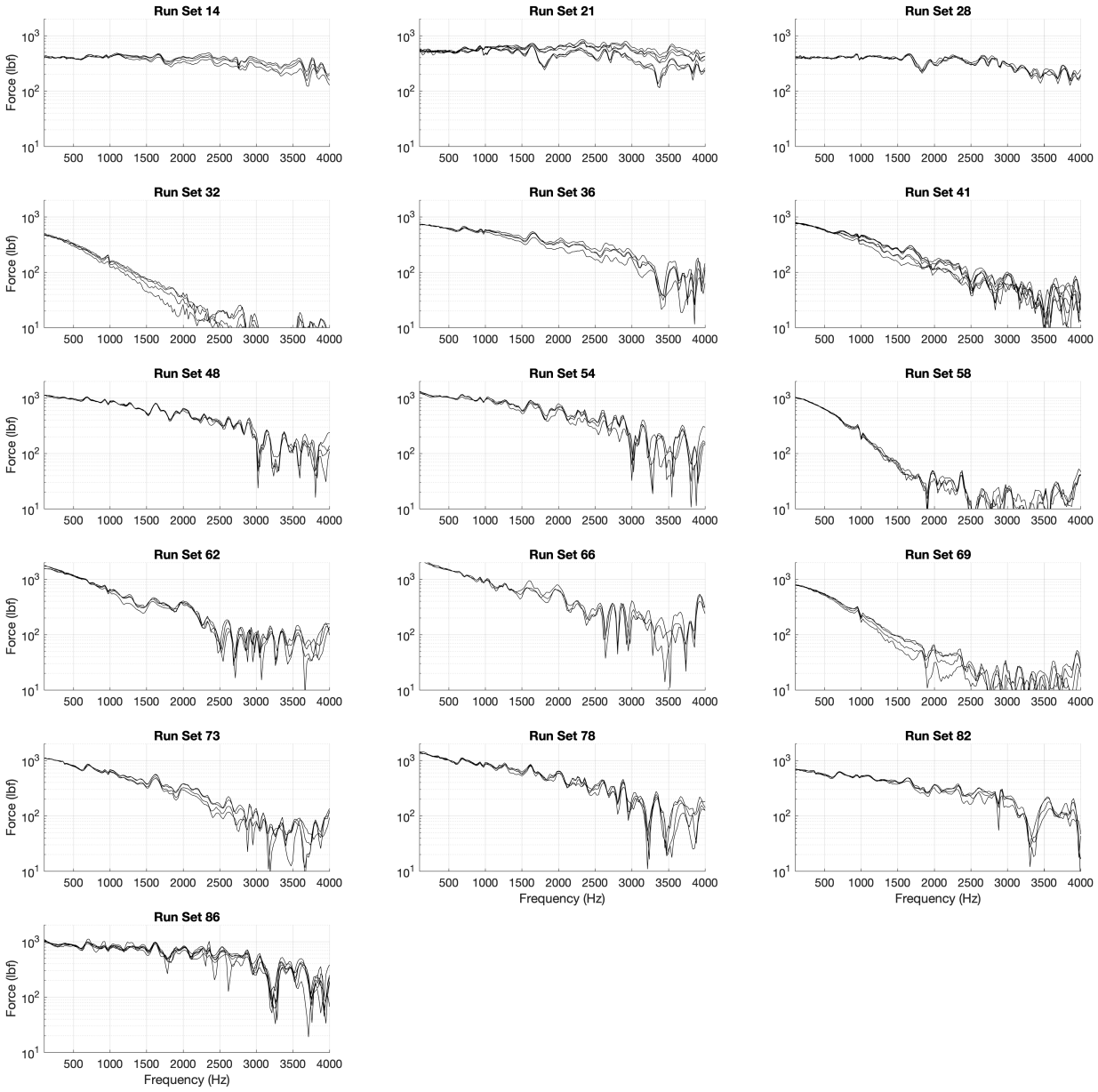

Figure 4: Forces in the frequency domain of all the test runs on the bare resonant plate with damping bars.

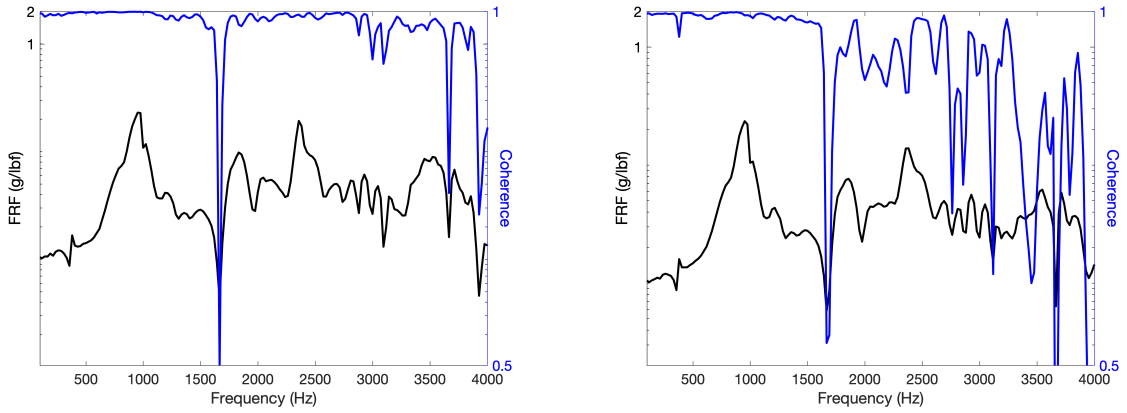

Figure 5: FRFs and coherence from the same set of test parameters (left), and from a low and high level impact (right)

Table 2: Comparison of modal damping levels from experimental modal tests and resonant plate shock tests. NF = Mode Not Found

Mode Number	Exp Modal Test Nat Freq (Damping)	Low Level Shock Nat Freq (Damping)	High Level Shock Nat Freq (Damping)
Mode 1 Frequency	391 Hz (0.35%)	379 Hz (0.41%)	383 Hz (0.40%)
Mode 2 Frequency	582 Hz (1.4%)	697 Hz (9.6%)	656 Hz (6.9%)
Mode 3 Frequency	1001 Hz (2.6%)	953 Hz (5.1%)	952 Hz (3.9%)
Mode 4 Frequency	1288 Hz (2.5%)	1167 Hz (4.5%)	NF
Mode 5 Frequency	2087 Hz (1.0%)	1822 Hz (4.0%)	NF
Mode 6 Frequency	2397 Hz (0.93%)	2359 Hz (1.2%)	NF

Finite element mode shapes with high Modal Assurance Criteria (MAC) values to the test shapes are in Figures 6 and 7. The frequency and damping comparisons of these modes are in Table 2. The table shows that there are some shifts in frequencies and damping of the different modes and that all modes are not affected the same with respect to the input load levels. This conclusion is expected, but predicting the shifts in frequency and damping is very difficult or impossible without data.

There are some difficulties in fitting the modal parameters from shock data. With the short time histories of the test, the frequency spacing in the FRFs is very high, about 24 Hz. This leads to the modal parameters being sensitive to small changes in the FRFs. The resynthesized complex mode indicator function (CMIF) of the low force input and high force input are in Figures 8 and 9 respectively. The resynthesis of the CMIF shows that the modes that are excited well are fit well to the test data. The resynthesized CMIFs also show that there are some modes indicated that are not fit well. Only modes fit with high confidence are included in the comparison shown in Table 2.

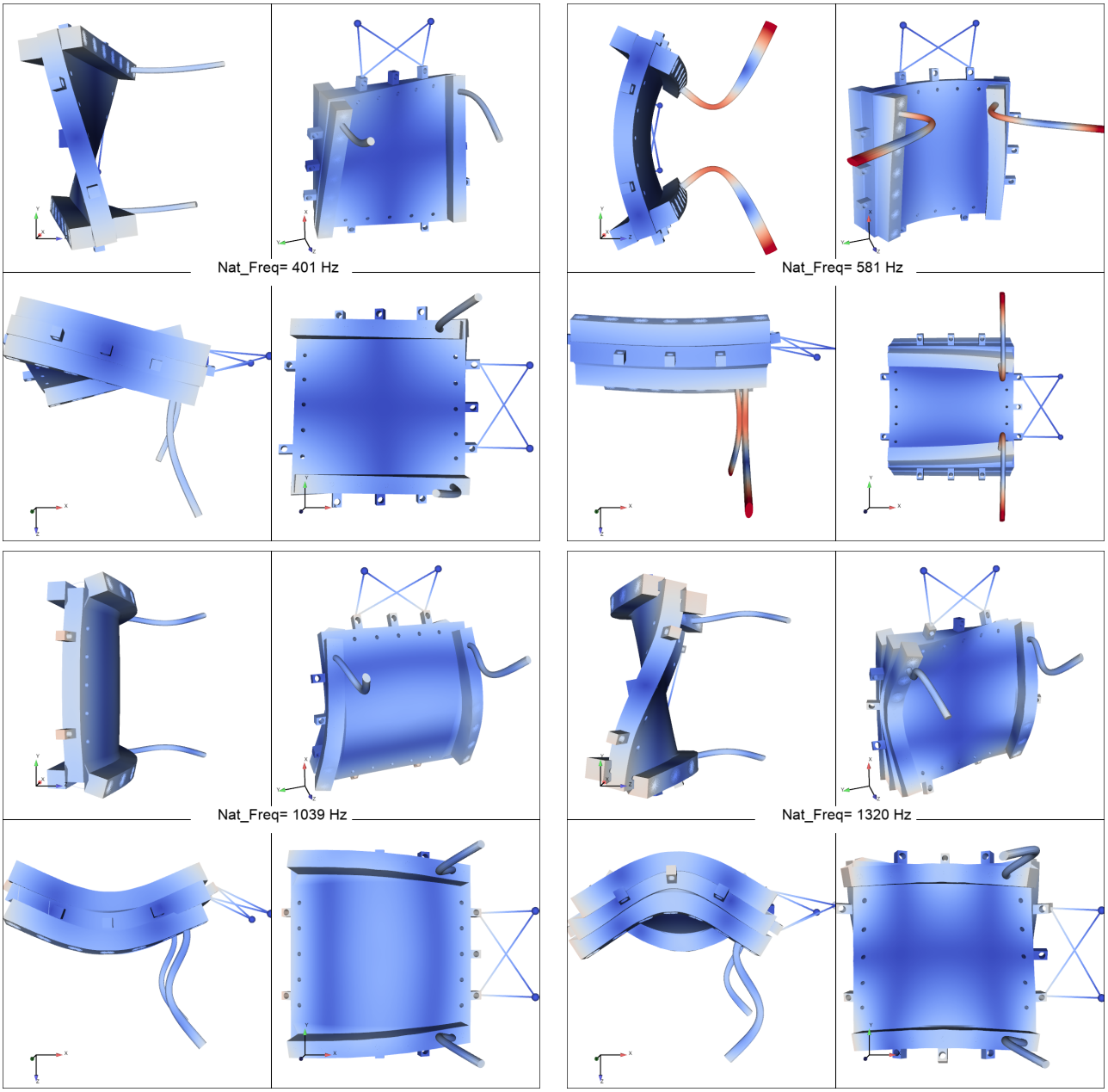

Figure 6: Mode shapes generated from a finite element model of test mode 1 (upper left), 2 (upper right), 3 (lower left), and 4 (lower right)

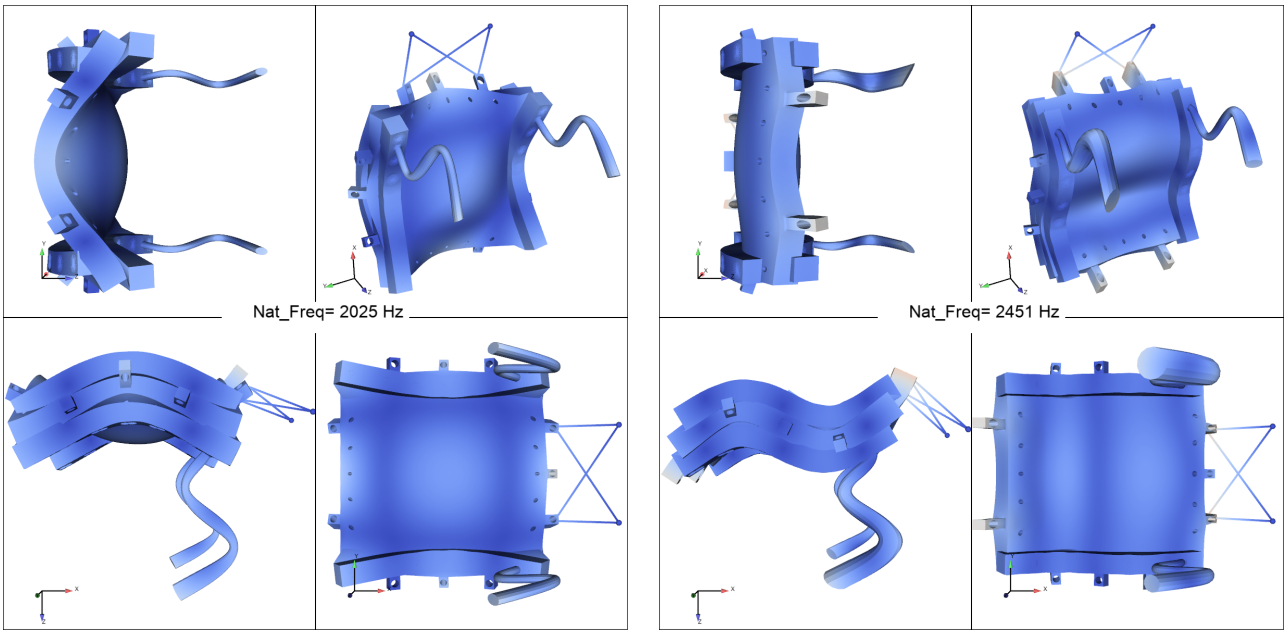

Figure 7: Mode shapes generated from a finite element model of test mode 5 (left) and 6 (right)

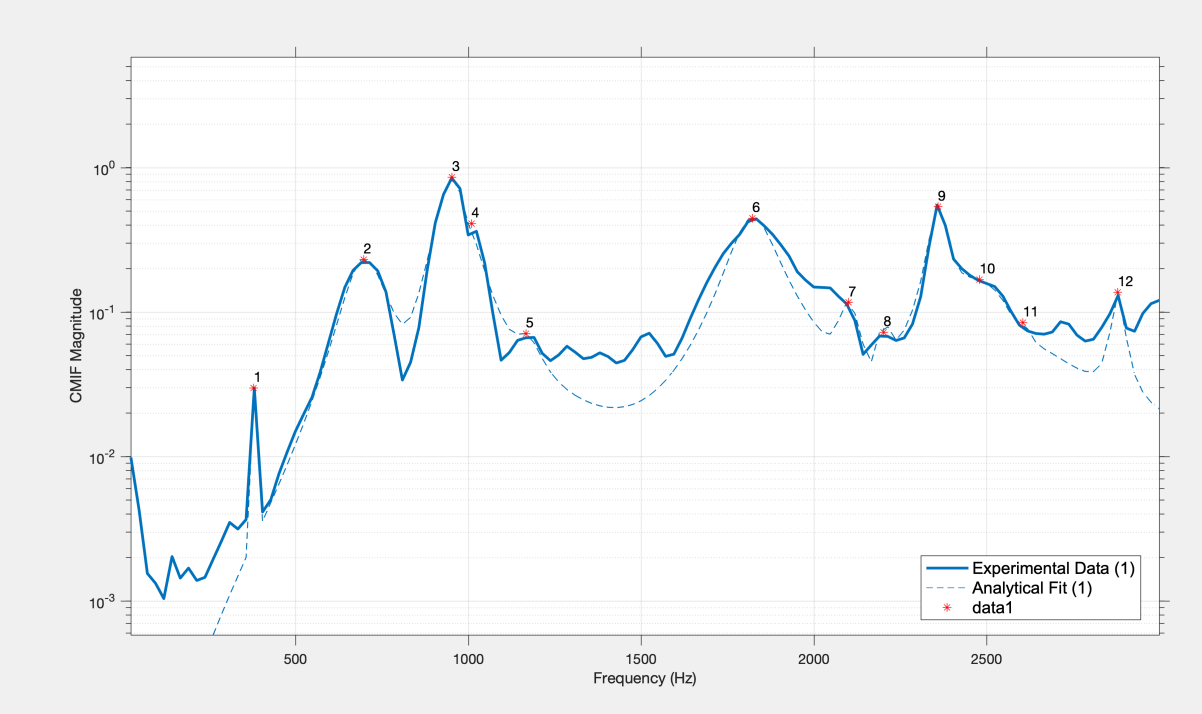

Figure 8: CMIF and resynthesized CMIF of the low level shock data

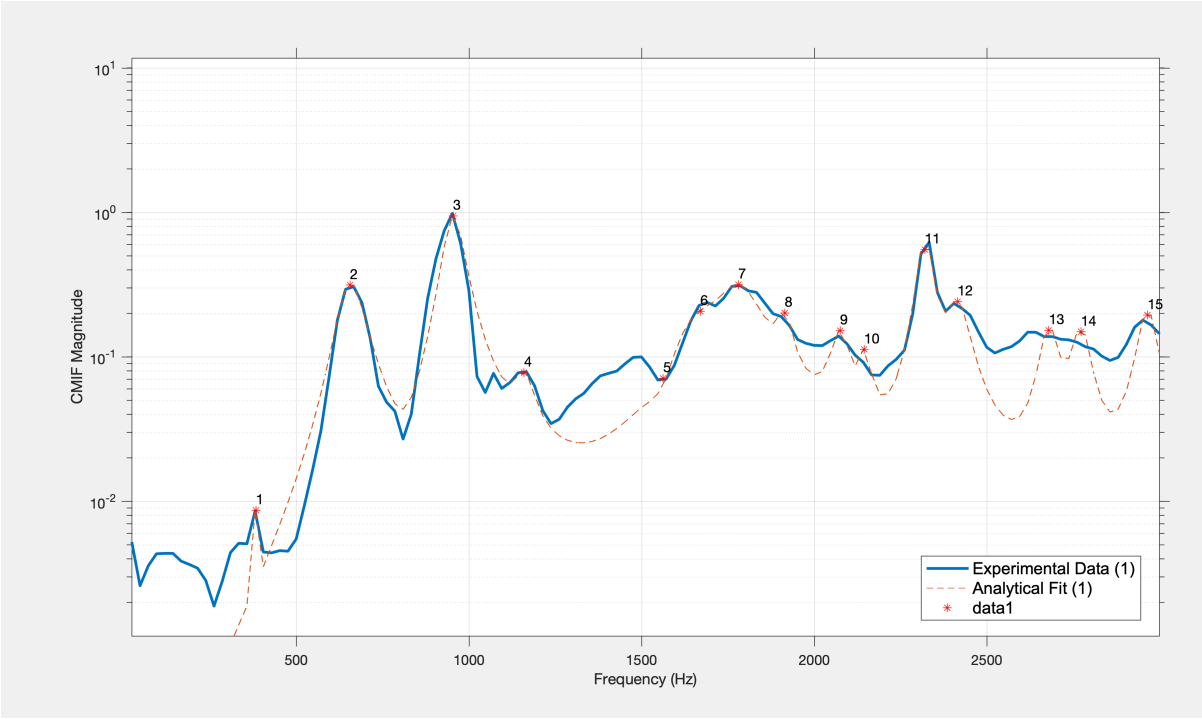

Figure 9: CMIF and resynthesized CMIF of the high level shock data

4 Conclusion

This paper demonstrates the process of executing the SWAT-TEEM algorithm on a resonant plate test and that the force calculated from a test can be used to generate FRFs of sufficient quality to fit modal parameters. Having quality FRFs provides insight in the linearity, the natural frequencies, the damping and the shapes of the test setup. The paper compares the modal parameters acquired at experimental modal levels, low level shocks, and high level shocks to demonstrate that the resonant plate has varying degrees of nonlinearities per mode. The results show that there are physics present in the system that prevent the system from behaving linearly with respect to input force. The nonlinearities present, however, do not prevent the use of a linearized model that is calibrated to the dynamics present at shock type input loads.

References

[1] Peter Avitabile. *Modal testing: a practitioner's guide*. John Wiley & Sons, 2017.

[2] Melih Eriten, Mehmet Kurt, Guanyang Luo, D Michael McFarland, Lawrence A Bergman, and Alexander F Vakakis. Nonlinear system identification of frictional effects in a beam with a bolted joint connection. *Mechanical Systems and Signal Processing*, 39(1-2):245–264, 2013.

[3] David J Ewins. *Modal testing: theory, practice and application*. John Wiley & Sons, 2009.

[4] Brian A Ferri and Ronald N Hopkins. *A Method for Determining Impact Force for Single and Tri Axis Resonant Plate Shock Simulations*, pages 65–71. Springer, 2020.

[5] Ward Heylen, Stefan Lammens, Paul Sas, et al. *Modal analysis theory and testing*, volume 200. Katholieke Universiteit Leuven Leuven, Belgium, 1997.

[6] Ronald Neil Hopkins and Carl Lee Sisemore. Design of a resonant plate shock test for simultaneous multi-axis excitation. Report SAND2019-0777C, Sandia National Lab.(SNL-NM), Albuquerque, NM (United States), 2019.

[7] Erica M Jacobson. *Using Frequency Based Substructuring to Optimize Multi-Axis Resonant Plate Shock Tests*. Thesis, 2019.

[8] Tyler F Schoenherr. Calculating the impact force of supersonic hail stones using SWAT-TEEM. In *Shock & Vibration, Aircraft/Aerospace, and Energy Harvesting, Volume 9*, pages 67–79. Springer, 2015.

[9] Carl Sisemore, Vit Babuska, and Robert Flores. Multi-axis resonant plate shock testing evaluation and test specification development. Report SAND2020-10224, Sandia National Lab.(SNL-NM), Albuquerque, NM (United States), 2020.